**Defense Threat Reduction Agency**
**8725 John J. Kingman Road, MS**
**6201 Fort Belvoir, VA 22060-6201**

**TECHNICAL REPORT**

# Experimental Research in Advanced Concepts for Novel Reactive Materials

Approved for public release; distribution is unlimited.

April 2013

Nick Glumac

Prepared by:
Mechanical Science &
Engineering Department
University of Illinois
Urbana-Champaign
1206 West Green St.
Urbana, IL 61801

# REPORT DOCUMENTATION PAGE

*Form Approved*
*OMB No. 0704-0188*

Public reporting burden for this collection of information is estimated to average 1 hour per response, including the time for reviewing instructions, searching existing data sources, gathering and maintaining the data needed, and completing and reviewing this collection of information. Send comments regarding this burden estimate or any other aspect of this collection of information, including suggestions for reducing this burden to Department of Defense, Washington Headquarters Services, Directorate for Information Operations and Reports (0704-0188), 1215 Jefferson Davis Highway, Suite 1204, Arlington, VA 22202-4302. Respondents should be aware that notwithstanding any other provision of law, no person shall be subject to any penalty for failing to comply with a collection of information if it does not display a currently valid OMB control number. **PLEASE DO NOT RETURN YOUR FORM TO THE ABOVE ADDRESS.**

| 1. REPORT DATE *(DD-MM-YYYY)* 00-04-2013 | 2. REPORT TYPE Technical | 3. DATES COVERED *(From - To)* |
|---|---|---|

| 4. TITLE AND SUBTITLE | 5a. CONTRACT NUMBER |
|---|---|
| Experimental Research in Advanced Concepts for Novel Reactive Materials | HDTRA1-12-1-0034 |
| | 5b. GRANT NUMBER |
| | 5c. PROGRAM ELEMENT NUMBER |

| 6. AUTHOR(S) | 5d. PROJECT NUMBER |
|---|---|
| Nick Glumac | 5e. TASK NUMBER |
| | 5f. WORK UNIT NUMBER |

| 7. PERFORMING ORGANIZATION NAME(S) AND ADDRESS(ES) | 8. PERFORMING ORGANIZATION REPORT NUMBER |
|---|---|
| University of Illinois Urbana-Champaign 1206 West Green Street Urbana, IL 61801 | |

| 9. SPONSORING / MONITORING AGENCY NAME(S) AND ADDRESS(ES) | 10. SPONSOR/MONITOR'S ACRONYM(S) |
|---|---|
| Defense Threat Reduction Agency 8725 John J. Kingman Road STOP 6201 Fort Belvoir, VA 22060 PM/S. Peiris | DTRA |
| | 11. SPONSOR/MONITOR'S REPORT NUMBER(S) DTRA-TR-13-20 |

**12. DISTRIBUTION / AVAILABILITY STATEMENT**

Approved for public release; distribution is unlimited.

**13. SUPPLEMENTARY NOTES**

**14. ABSTRACT**

This proposed research addressed two areas of reactive materials (RM) research that can potentially improve DoD capabilities for defeat of WMDs. The first concept seeks to enhance feasibility of weaponizing RMs by researching a novel route to the production of metal-matrix composite RM casings and liners - infiltration of dense inert fibrous grids (e.g W wire) with castable lighter energetic metals (e.g. Al). This approach would potentially yield a route to practical, cost-effective production of non-porous, highly energetic, high density RM liners and cases with high strength and stiffness. Such an approach would be a great improvement in cost over the powder-based techniques currently envisioned - greatly speeding implementation.

**15. SUBJECT TERMS**

energetic case    reactive materials    infiltration casting

| 16. SECURITY CLASSIFICATION OF: | | | 17. LIMITATION OF ABSTRACT | 18. NUMBER OF PAGES | 19a. NAME OF RESPONSIBLE PERSON Suhithi Peiris |
|---|---|---|---|---|---|
| a. REPORT | b. ABSTRACT | c. THIS PAGE | SAR | 28 | 19b. TELEPHONE NUMBER *(include area code)* |
| Unclassified | Unclassified | Unclassified | | | 703-767-4732 |

**Standard Form 298 (Rev. 8-98)**
Prescribed by ANSI Std. Z39.18

# CONVERSION TABLE

Conversion Factors for U.S. Customary to metric (SI) units of measurement.

MULTIPLY────────────────▶ BY ────────────────▶ TO GET

TO GET ◀──────────────── BY ◀──────────────── DIVIDE

| | | |
|---|---|---|
| angstrom | $1.000\ 000 \times E\ -10$ | meters (m) |
| atmosphere (normal) | $1.013\ 25\ \ \times E\ +2$ | kilo pascal (kPa) |
| bar | $1.000\ 000 \times E\ +2$ | kilo pascal (kPa) |
| barn | $1.000\ 000 \times E\ -28$ | meter$^2$ (m$^2$) |
| British thermal unit (thermochemical) | $1.054\ 350 \times E\ +3$ | joule (J) |
| calorie (thermochemical) | $4.184\ 000$ | joule (J) |
| cal (thermochemical/cm$^2$) | $4.184\ 000 \times E\ -2$ | mega joule/m$^2$ (MJ/m$^2$) |
| curie | $3.700\ 000 \times E\ +1$ | *giga bacquerel (GBq) |
| degree (angle) | $1.745\ 329 \times E\ -2$ | radian (rad) |
| degree Fahrenheit | $t_k = (t°f + 459.67)/1.8$ | degree kelvin (K) |
| electron volt | $1.602\ 19\ \ \times E\ -19$ | joule (J) |
| erg | $1.000\ 000 \times E\ -7$ | joule (J) |
| erg/second | $1.000\ 000 \times E\ -7$ | watt (W) |
| foot | $3.048\ 000 \times E\ -1$ | meter (m) |
| foot-pound-force | $1.355\ 818$ | joule (J) |
| gallon (U.S. liquid) | $3.785\ 412 \times E\ -3$ | meter$^3$ (m$^3$) |
| inch | $2.540\ 000 \times E\ -2$ | meter (m) |
| jerk | $1.000\ 000 \times E\ +9$ | joule (J) |
| joule/kilogram (J/kg) radiation dose   absorbed | $1.000\ 000$ | Gray (Gy) |
| kilotons | $4.183$ | terajoules |
| kip (1000 lbf) | $4.448\ 222 \times E\ +3$ | newton (N) |
| kip/inch$^2$ (ksi) | $6.894\ 757 \times E\ +3$ | kilo pascal (kPa) |
| ktap | $1.000\ 000 \times E\ +2$ | newton-second/m$^2$ (N-s/m$^2$) |
| micron | $1.000\ 000 \times E\ -6$ | meter (m) |
| mil | $2.540\ 000 \times E\ -5$ | meter (m) |
| mile (international) | $1.609\ 344 \times E\ +3$ | meter (m) |
| ounce | $2.834\ 952 \times E\ -2$ | kilogram (kg) |
| pound-force (lbs avoirdupois) | $4.448\ 222$ | newton (N) |
| pound-force inch | $1.129\ 848 \times E\ -1$ | newton-meter (N-m) |
| pound-force/inch | $1.751\ 268 \times E\ +2$ | newton/meter (N/m) |
| pound-force/foot$^2$ | $4.788\ 026 \times E\ -2$ | kilo pascal (kPa) |
| pound-force/inch$^2$ (psi) | $6.894\ 757$ | kilo pascal (kPa) |
| pound-mass (lbm avoirdupois) | $4.535\ 924 \times E\ -1$ | kilogram (kg) |
| pound-mass-foot$^2$ (moment of inertia) | $4.214\ 011 \times E\ -2$ | kilogram-meter$^2$ (kg-m$^2$) |
| pound-mass/foot$^3$ | $1.601\ 846 \times E\ +1$ | kilogram-meter$^3$ (kg/m$^3$) |
| rad (radiation dose absorbed) | $1.000\ 000 \times E\ -2$ | **Gray (Gy) |
| roentgen | $2.579\ 760 \times E\ -4$ | coulomb/kilogram (C/kg) |
| shake | $1.000\ 000 \times E\ -8$ | second (s) |
| slug | $1.459\ 390 \times E\ +1$ | kilogram (kg) |
| torr (mm Hg, 0$^0$ C) | $1.333\ 22\ \ \times E\ -1$ | kilo pascal (kPa) |

 *The bacquerel (Bq) is the SI unit of radioactivity; 1 Bq = 1 event/s.
 **The Gray (GY) is the SI unit of absorbed radiation.

# I. Project Overview

This proposed research addressed two areas of reactive materials (RMs) research that can potentially improve DoD capabilities for defeat of WMDs. The first concept seeks to enhance feasibility of weaponizing RMs by researching a novel route to the production of metal-matrix composite RM casings and liners - infiltration of dense inert fibrous grids (e.g W wire) with castable lighter energetic metals (e.g. Al). This approach would potentially yield a route to practical, cost-effective production of non-porous, highly energetic, high density RM liners and cases with high strength and stiffness. Such an approach would be a great improvement in cost over the powder-based techniques currently envisioned - greatly speeding implementation.

The second concept builds on recent research on a speculative energy state of hydrogen, which, if attainable, would allow munitions to achieve greater than 10-fold increase in energy density over current chemical approaches. The theory and experiments speculate on accessible states of hydrogen with principle quantum number values of *1/n*. While highly speculative in nature, the experimental evidence published in many mainstream physics journals is compelling, and the potential impact here is disruptive. Therefore, an independent verification of these results is worthwhile, and such an experiment was completed during the research period. These experiments involved the electronic spectrum in the vacuum ultraviolet of the proposed di-hydrino molecule.

## I.A. Objectives
This project had two major objectives:

1) Demonstrate the novel approach of infiltration casting to produce structural energetic materials viable for case applications.

2) Attempt validation of a key experiment that suggests that a novel state of molecular hydrogen – with two hydrogen atom in quantum states below the currently accepted ground state – exists. Provide a detailed and high resolution analysis of this spectrum with investigations into the roles of possible impurities and spurious signals.

Both objectives were achieved during the project period (April – October 2012). Results will be reported in two parts sequentially.

# II. Results

## II.A Infiltration Casting

## II.A.1 Background
Reactive materials (RMs) represent an active area of research in the Department of Defense. Current methodologies for producing RM cases and liners involve

primarily powder based methods where reactants are combined as powders (e.g. in the MIC materials and mechanically alloyed composites). Consolidation is expensive and challenging on complex geometries. Casting, however, is cheap and mature technology. The premise of this research is that if a casting technology could produce high performing RM cases, then weaponization of RM technology would be greatly facilitated. Our approach was based on an idea provided by Dr. Kibong Kim to infiltrate aluminum into tungsten matrices in the casting process, producing dense and energetic materials.

## II.A.2  Preparation and Fabrication Methods
Multiple densification methods were tested using various forms of tungsten in order to determine if an ideal casing construction method could be defined. The forms of tungsten used during experimentation are as follows:
- 50 μm diameter tungsten wire
- 0.010" diameter tungsten wire
- 0.020" diameter tungsten wire
- 0.025" diameter tungsten wire
- 0.032" diameter tungsten wire
- 2 mm diameter tungsten spheres
- 4 mm diameter tungsten spheres
- 150-300 μm diameter tungsten powder

The methods used to create the casings include the following, each of which is outlined below:
- Experimental casting in a small furnace
- Sand casting
- Sand casting with pre-cast heating of tungsten elements
- Induction casting with applied pressure

## II.A.2.a Experimental Furnace Casting
The developmental casting in the furnace was performed as a preliminary investigation of aluminum infiltration around tungsten elements before moving to larger scale sand casting techniques. Each preliminary test was performed in the furnace at a temperature of 950 °C for a period of approximately half an hour. The furnace consisted of an environmental chamber with resistive heating elements, and the temperature could be controlled to within 1 °C up to 1000 °C. The small size of the furnace limited us to samples below 2 inches in diameter. The first attempt at infiltration consisted of aluminum melted around 0.010" diameter tungsten wire pieces, as shown in Figure 1 below:
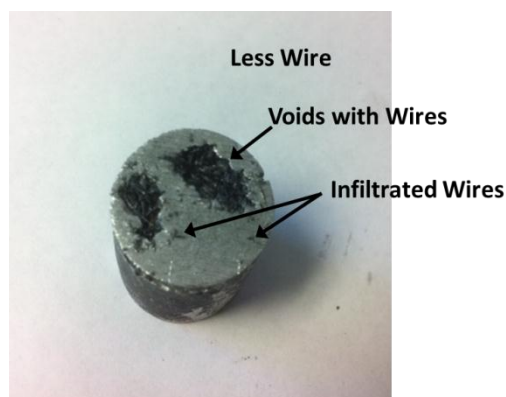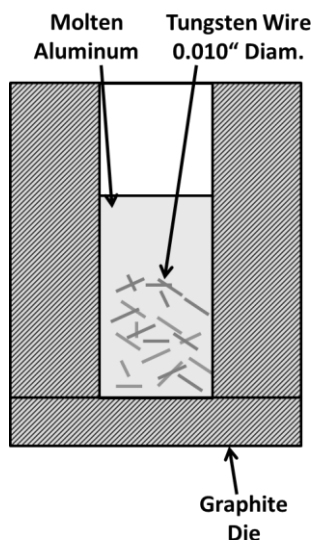
**Figure 1: Tungsten wire pieces in aluminum in an environmental casting furnace at 950 °C.  Sample diameter is 0.5 inches.**

Some of the wires were infiltrated, yet some left voids where the wire pieces grouped together to form pockets that could not be infiltrated by the aluminum. The next attempt was a similar test using tungsten powder. The method and end result is shown below in Figure 2:
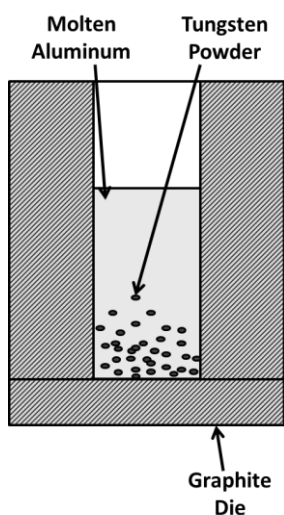


**Figure 2: Tungsten powder in aluminum in a casting furnace at 950 C.**

The results of the tungsten powder test were similar to that of the wire pieces test. Some of the powder was infiltrated by the aluminum while some of the powder

agglomerated, leaving void pockets in the sample. It is important to note the voids created on the outer diameter of the work piece, as these were regions with high possibility of failure due to the crumbling nature of the powder in these areas. However, the increase in density was noticeable when using the tungsten powder.

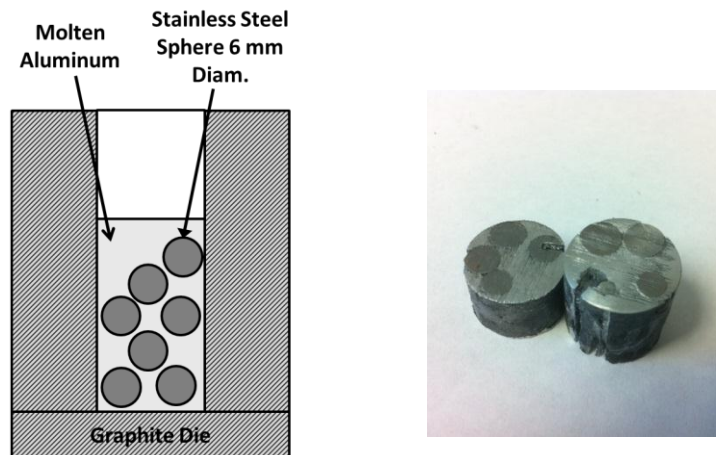High density spheres were also tested. The preliminary tests used stainless steel spheres that were on hand, and the results of a sphere test are shown below:



**Figure 3: Spheres in aluminum at 950 C.**

The spheres, which are considerably larger than the wire and powder, allowed for more infiltration while at the same time increasing densification over the other materials tested. There were no voids found in this sample, indicating "wetting" of the tungsten surface and full infiltration between the spheres. Small diameter (50 micron) tungsten wire was also tested in the furnace, but the infiltration was poor as will be shown in succeeding figures.

**II.A.2.b  Sand Casting**
After completion of the small furnace testing, larger scale sand-casting was then performed in an open face mold by pouring molten aluminum at ≈790 ℃ onto tungsten wires located inside the mold.  In this process, the mold is prepared, the wires are inserted into the mold, and the crucible of liquid aluminum is poured into the mold.  No external pressure was applied, and the cooling of the material was limited primarily by the mold material.  A sample schematic of this process is shown in the figure below:
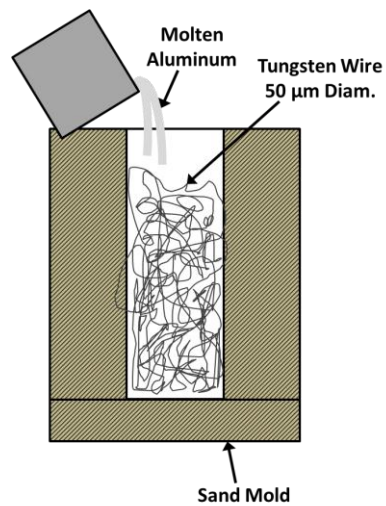
**Figure 4: Schematic of open face sand mold with tungsten wire. Pouring temperature was 790 °C.**

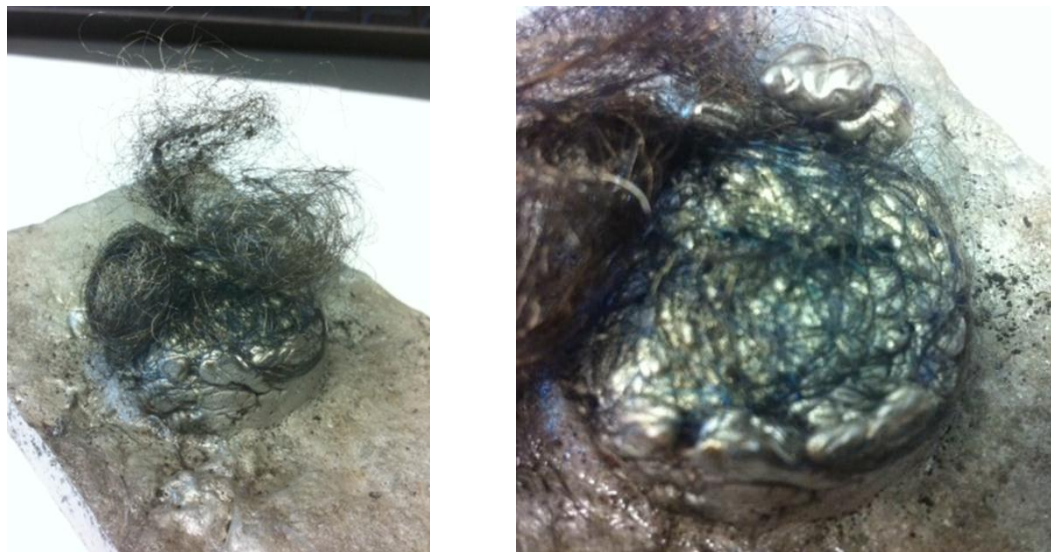The results of this wire infiltration test are shown below:



**Figure 5: 50 μm diameter tungsten wire casting results from the process depicted in Figure 4.**

These results show that the small diameter wire is not ideal for the sand casting method of production. The surface area of the wires is large enough to cool the

aluminum before it reaches the bottom of the mold and therefore infiltration is nearly impossible using this particular method.

A sand core was added to the mold to create a casing annulus and 6 mm diameter stainless steel spheres (used earlier) were added to the mold before pouring. The results are shown in Figure 6.



**Figure 6: Stainless steel sphere casting results.  Pouring at 790 °C.  Standard annular sand casting mold.**

**II.A.2.c  Heated Sand Casting**
The results from preliminary casting showed that achieving infiltration around the tungsten elements was difficult and another approach needed to be considered. The next approach implemented cored sand casting in a closed sand mold with preheating of tungsten elements prior to pouring the molten aluminum. The cases tested were a wrap of 0.010" diameter tungsten wire, a wrap of 0.025" tungsten wire, and 4 mm diameter tungsten spheres.  Each of these tests used a propane torch to heat the elements in the mold prior to pouring. The results of this casting procedure are detailed below:



**Figure 7: 0.010" diameter tungsten wire cast.  Preheated mold and tungsten wires before pouring at 790 C.**

**Figure 8: 0.025" diameter tungsten wire cast. Preheated mold and tungsten wires before pouring at 790 C.**



**Figure 9: 4 mm diameter tungsten sphere cast. Preheated mold and tungsten spheres before pouring at 790 C.**

Through the second casting iteration it was determined that heating the tungsten elements prior to pouring immensely improved aluminum infiltration. Pre-heating the 50 μm tungsten wire was not practical due to the amount of wire that needed to be heated and the amount of oxidation that occurred while heating. The casings created during this procedure, though slightly incomplete, were structurally sound and much denser than a pure aluminum casing of comparable size. While this method seemed to hold promise, mold preparation and casting lab procedures made for a lengthy process. It was now confirmed that heating the tungsten elements *while* casting would create an even more ideal process and further increase infiltration.

### II.A.2.d  Induction Casting
The next method of casing preparation combined the necessary requirements found using previous attempts by implementing an induction heater to heat both the aluminum and the tungsten at the same time under pressure, thereby encouraging the highest amount of infiltration using a relatively faster process. A 15kW high-frequency induction heater was purchased and installed in the laboratory. In order to create new casings in an efficient manner, a reusable, graphite mold was machined to hold the aluminum and tungsten during heating. The mold was created in four pieces: a base, a core, a sleeve, and a pressure rod. The graphite mold is shown in Figure 10.



**Figure 10: Graphite mold, (L) Disassembled, (R) Assembled**

The induction heater provides a variable output frequency of 30-100 kHz, giving a heating current of 200-600 A through a separated transformer head unit. The induction heater setup is shown below:
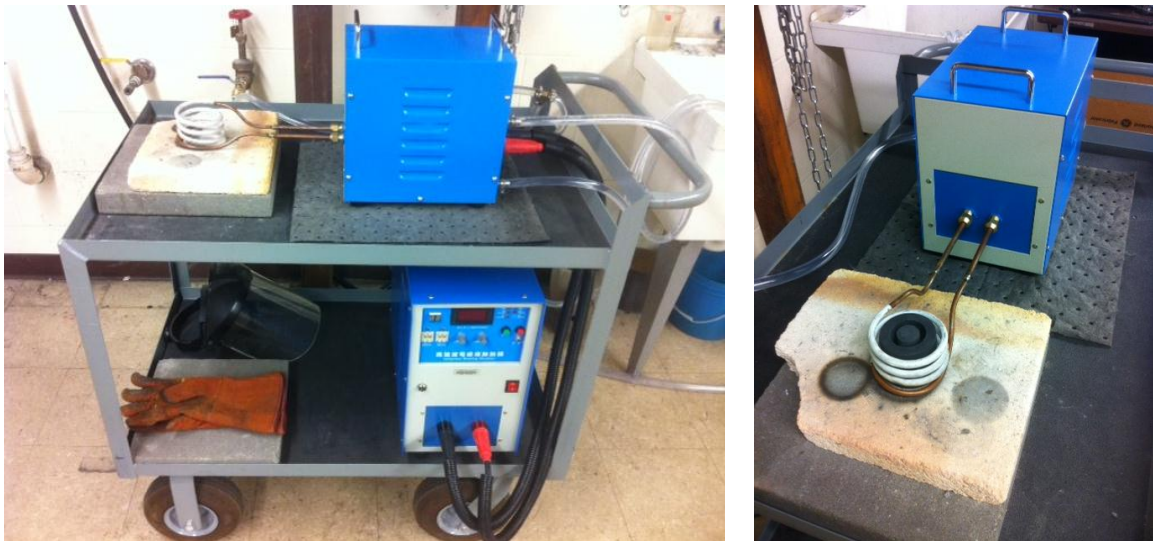


**Figure 11: Induction heater and casting arrangement**

*Any opinions expressed in this document are those of the author alone and do not necessarily represent the opinions of the University of Illinois or DTRA.*

Utilizing the displayed arrangement, a more efficient method was established for creating aluminum casings and testing the infiltration potential of various forms of tungsten elements. A successful method of casing creation began with wrapping tungsten wire into a cylindrical shape that held its form. The ability of the wire wrap to hold its shape is vital in the densification process, as it must remain intact in the mold under applied pressure. Aluminum was then melted in the graphite mold by means of induction heating, and the wire wrap was inserted into the molten aluminum. The pressure rod applied a compression force to the molten aluminum to enhance the infiltration around the tungsten wires. During application of the pressure force, the induction process heated both the tungsten wires and the aluminum, which helps increase infiltration as shown in the sand casting experiments. Images of the tungsten wire wrap and an example of the infiltration possible using induction casting are shown below. The dark color on the inside of the casing is due to residual graphite from the mold.
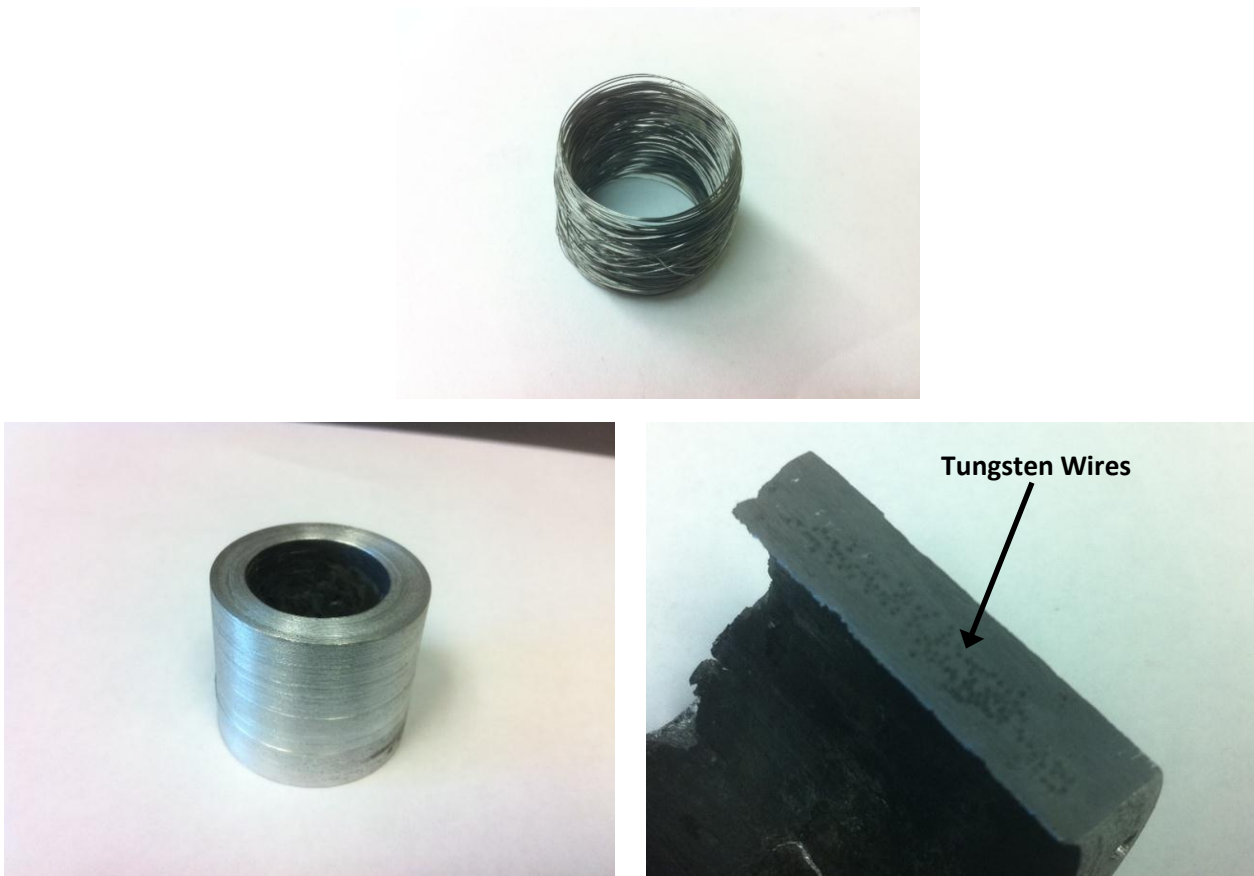


**Figure 12: (Top) Tungsten wire wrap using 0.010" diameter wire, (Left) Al/W casing created using induction casting, (Right) Aluminum infiltration around tungsten wire wrap**

Tungsten wires of 0.010", 0.020", and 0.032" diameter were tested to determine their ability to increase the density of a pure aluminum casing. The 0.020" wire,

when wrapped as described above, gave the highest percentage of tungsten of any of the wire wraps. The amount of 0.010" wire needed to match this density was large and made infiltration between wires more difficult. The 0.032" wire was acquired to create a wire wrap, but it was seen that any wire diameters above the 0.020" diameter would not easily wrap and would break readily. Instead, the 0.032" diameter tungsten wire was cut into pieces approximately 0.75" long, in order to create a more traditional metal-matrix composite. The wires were oriented vertically in the mold and aluminum was melted around the top and bottom of the wires using induction heating. This process created a casing which had small areas where infiltration was scarce along the outer diameter, but infiltration on the inside of the casing was fully accomplished.

Other tungsten elements were tested using the induction casting method, but none proved as successful as the wire. Both powder and small tungsten pieces were not capable of being easily distributed throughout the aluminum matrix, causing large voids and structural weaknesses where the elements were clumped together. The tungsten spheres appeared to work at first and provided casings with approximately 65% tungsten by mass. However, after complete cooling, cracks were seen to form and the casings could essentially be pulled apart by hand. This cracking is likely due to the difference between each material's coefficient of thermal expansion. With such a high amount of tungsten present within the aluminum, the difference in thermal expansion is enough to generate severe dislocations within the metal matrix, especially at the interface between the tungsten spheres and the aluminum. If a slower cooling process of the casing could be controlled after casting, the tungsten spheres would provide a viable option for densifying the aluminum. This task has not yet been fully investigated using the induction casting method, but is something to be researched in the near future.

**Explosive Initiation of Casings**
Once increased density was achieved with tungsten wires using the induction casting method, four densified casings were explosively initiated in the blast chamber located at UIUC to determine the role that the tungsten elements play in the reaction performance of the casings. The characteristics of each casing tested are outlined in Table 1, while photographs of each densified casing are also shown in Figure 13. It is important to note that Tests 1, 2, and 3 were casings with tungsten wire wraps, while Test 4 was created using the metal-matrix composite technique with vertical tungsten wire strips.

**Table 1: Casing Characteristics**

| Test | Material | Mass (g) | Volume (cm³) | Density (g/cm³) | % Tungsten by Mass |
|------|----------|----------|--------------|-----------------|---------------------|
| A | Aluminum 6061 | 31.71 | 11.89 | 2.67 | 0 |
| S1 | Stainless 304 | 39.43 | 5.07 | 7.78 | 0 |
| 1 | Al + 0.01" W Wrap | 45.32 | 12.32 | 3.68 | 30.92 |
| 2 | Al + 0.02" W Wrap | 56.64 | 12.38 | 4.57 | 47.65 |
| 3 | Al + 0.02" W Wrap | 66.82 | 12.83 | 5.21 | 56.04 |
| 4 | Al + 0.032" W Matrix | 73.12 | 12.85 | 5.69 | 61.09 |
| 5 | Al+0.051" W Matrix | 102.34 | 11.09 | 9.22 | 82.26 |



**Figure 13: Clockwise from top: 30.92% W casing, 47.65% W casing, 61.09% W casing, 56.04% W casing**

**Figure 14:  Three photographs of the densest casing produced (9.2 g/cc) with 82% W by mass.**

Each reactive casing was explosively initiated using 10 g of PBXN-9 and one RP-80 EBW detonator. During each test, the diagnostics performed included two transient pressure measurements, two quasi-static pressure (QSP) measurements, high speed imaging, and time-resolved imaging spectroscopy. Both transient pressure measurements provided initial blast wave side-on pressures as well as a long-duration QSP measurement. The four total QSP results for each test were consistent with one another and were averaged together.   The QSP can be directly related to the energy release of the RM sample and explosive according to the relation:

$$\Delta P_{QSP} = \frac{\gamma - 1}{V} \Delta E$$

where ΔE is the energy release, γ is the specific heat ratio, and V is the chamber volume.

The figure below shows an example of the casing test setup in the blast chamber. The high explosive sits inside the casing and the detonator is inserted through the steel cap on the top.

Each test was referenced to a stainless steel (type 304) inert casing as a baseline which produced a QSP value of 0.78 psi. This value was then subtracted from the casing values to yield a net QSP produced by the casing alone. The mass of the inert casing was approximately the same as the baseline aluminum case tested. The QSP

results are shown below in Table 2. Each net QSP value can provide a specific energy release of the reactive casing based on a constant volume ideal gas analysis. The theoretical energy release (enthalpy of combustion) of aluminum with oxygen is calculated to be -31.05 kJ/g. This value is used to determine a percent theoretical energy release from the experimentally determined values.
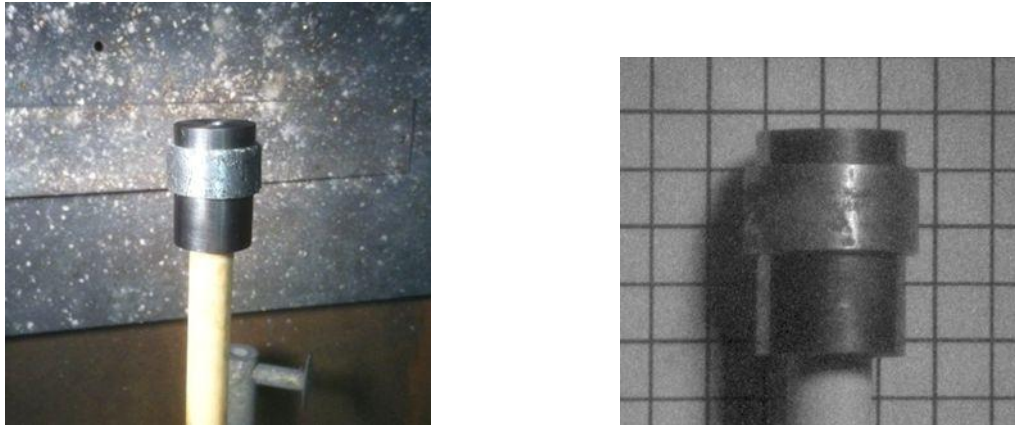


**Figure 15: (L) Photograph showing casing test setup,(R) Pre-test optical calibration with ½" x ½" grid arrangement**

**Table 2: QSP and Energy Release Results**

| Test | Material | Mass (g) | Mass of Aluminum (g) | Net QSP (psi) | Specific Energy Release (kJ/g) | % Theoretical Energy Release |
|------|----------|----------|----------------------|---------------|--------------------------------|------------------------------|
| A | Aluminum 6061 | 31.71 | 31.71 | 2.64 | 2.60 | 8.38 |
| 1 | Al + 0.01" W Wrap | 45.32 | 31.31 | 3.63 | 3.63 | 11.68 |
| 2 | Al + 0.02" W Wrap | 56.64 | 29.65 | 3.15 | 3.32 | 10.68 |
| 3 | Al + 0.02" W Wrap | 66.82 | 29.37 | 2.51 | 2.68 | 8.62 |
| 4 | Al + 0.032" W Matrix | 73.12 | 28.45 | 3.43 | 3.77 | 12.14 |
| 5 | Al + 0.051" W Matrix | 102.34 | 18.16 | 2.84 | 4.90 | 15.77 |

As seen in the table above, each of the densified casings outperformed the pure aluminum casing. For the wire wrap casings, the tests showed that as the amount of tungsten was increased from 30.92% to 56.04%, the specific energy release decreased. However, these cases had less aluminum and still outperformed the pure aluminum casing. It appears that as the pure aluminum case interacts with the HE blast wave it tends to create large fragments that do not fully react before being ejected from the blast. For the cases with tungsten contained in them, the HE blast wave interacts with the infiltrated tungsten to create regions where the aluminum is broken into finer fragments that react more fully and encourage further local

reaction. The experiments also show a difference between the wire wrap and the metal-matrix composite forms tested. The trend of decreasing specific energy release with increasing density is interrupted by the vertical tungsten wire casing (Test 4) and then the densest sample (Test 5). This enhanced efficiency is believed to be due to the fact that the tungsten and aluminum are more uniformly distributed throughout the Test 4 and Test 5 casings. The wire wrap casings were fully infiltrated, but the amount of aluminum between the wrap layers varied. The wire wrap casings also had more aluminum on the edges that was not in contact with the tungsten. This may have caused more large fragmentation in Tests 1, 2, and 3 than in Test 4 and Test 5. The Test 4 vertical wire matrix allowed for the tungsten to be more evenly distributed amongst the aluminum, thereby encouraging finer fragmentation of aluminum and more reaction. Figure 16 below compares the imaging for each of the tests mentioned above. Each row corresponds to its test number on the left.
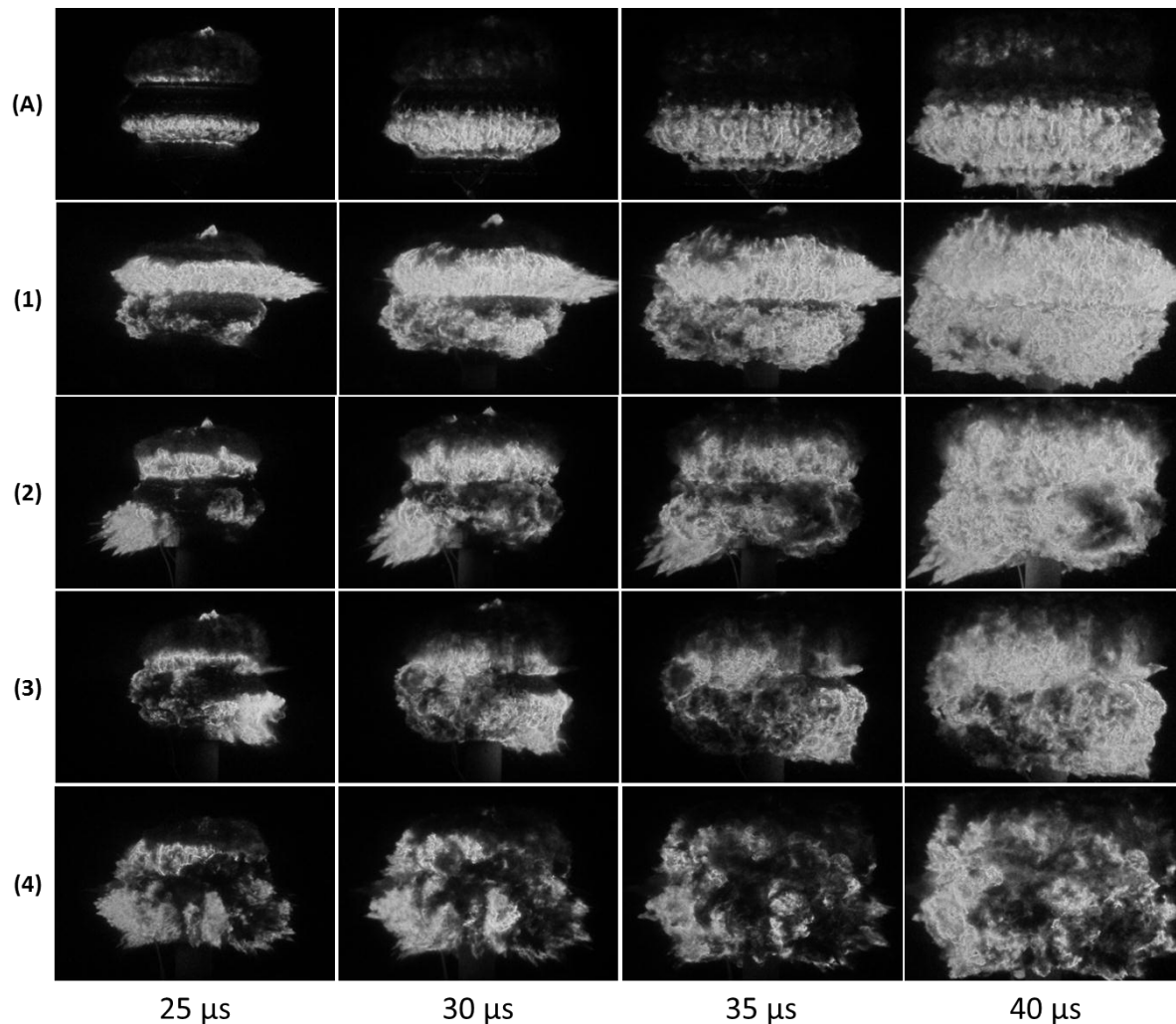


**Figure 16: Image comparison of reactive casing tests**

The imaging results show the same trend as the measured QSP values – namely, the 30.92% tungsten casing (Test 1) visually displays the highest amount of reaction, followed by Test 2 then Test 3. The Test 4 reaction cloud appears to be less confined at any given time, indicating that the aluminum in the casing is more readily breaking apart even at the early initiation times.

Time-resolved imaging spectroscopy was also captured for each of the high speed images. The spectral signatures of the casings were primarily dominated by the emission of aluminum monoxide. The spectrum below is an example of what the image is reduced to when examined using a custom analysis code. The spectra from the reactive casing tests were all very similar in nature, exhibiting the AlO vibrational bands with varying intensity depending on the amount of reaction. The strong atomic peak around 521 nm was seen in each test and is due to the chromium in the steel base and cap that held the casing in place.
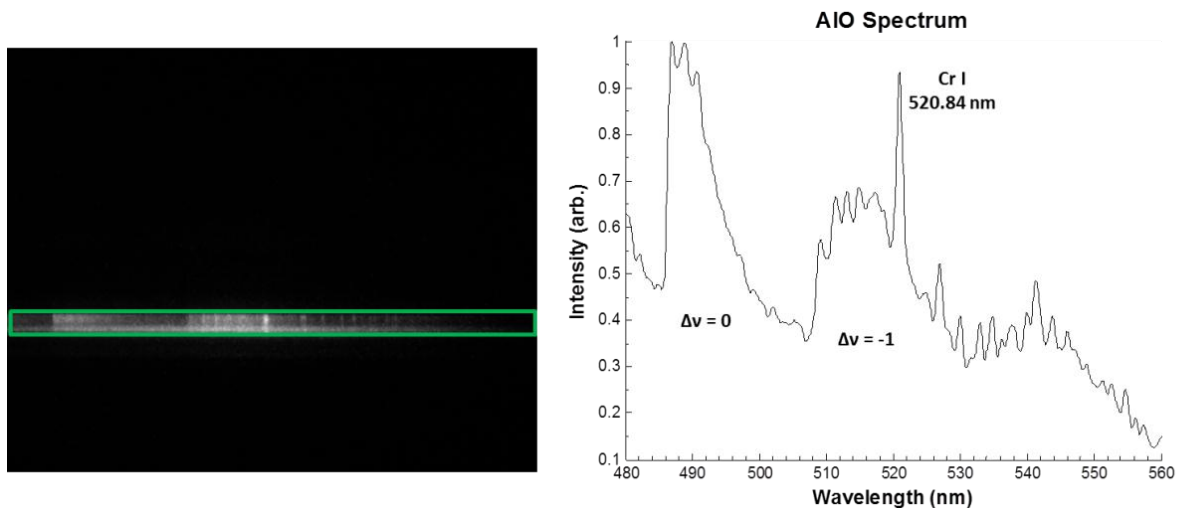


**Figure 17: (L) Spectrum Image, (R) Reduced spectrum showing AlO vibration bands**

**Summary and Recommendations**

Through testing of various manufacturing methods, it was shown that tungsten wires (particularly larger diameters) and tungsten spheres have the highest potential for increasing the density of reactive aluminum casings. The induction casting method shows the most promise as a manufacturing technique for densified casings due to its lower cost of operation, relatively faster processing speeds, and ability to heat both tungsten and aluminum while casting. The induction casting method also allows for discretion of which tungsten element will be added to the casing, providing yet another means for customizing casings based on warfare needs.

It was determined experimentally that the tungsten wire is difficult to work with by hand, but would not be as difficult if implemented in, for example, a wire spinning

manufacturing process. Aluminum infiltration around tungsten wires is not easily achieved by any other method besides induction casting and the cost of the wires is relatively high compared to other forms of tungsten. The tungsten spheres are an interesting possibility for densification and provide not only the highest percentage of tungsten by mass seen in these experiments, but also present a possible enhanced damage mechanism due to the ejection of the spheres upon casing initiation. The spheres are simple to implement and have a relatively low cost (on the order of $60 per pound). However, further work needs to be performed with the spheres to determine an appropriate cooling process to discourage dislocation formation.

Based on the processes described above, a manufacturing method which implements induction casting is recommended. Die casting of aluminum is a mature process that can be readily modified to produce densified aluminum casings. The die design is relatively simple and the die can be coated with a lubricant for easy removal of the casing. A refractory material could also be implemented for the die construction. Once the die is prepared, aluminum is melted within the die by means of induction heating. When the aluminum is fully molten, the tungsten elements are inserted into the die and are heated for a short time with the aluminum. The tungsten heats faster than the aluminum under induction heating due to its higher electrical resistivity. Pressure is then applied to the molten aluminum to encourage more infiltration around the tungsten. The applied pressure may be accomplished various ways, whether through direct application using a ram or through the use of a high-pressure, inert gas. Once the aluminum has solidified, the casing is removed from the mold for further cooling and the process is repeated. Another possibility for manufacturing is to preheat the tungsten in the mold and then pour molten aluminum into the die. This process would be more akin to a traditional die casting method and may be suitable for densification techniques like the metal-matrix composite with vertical tungsten wires.
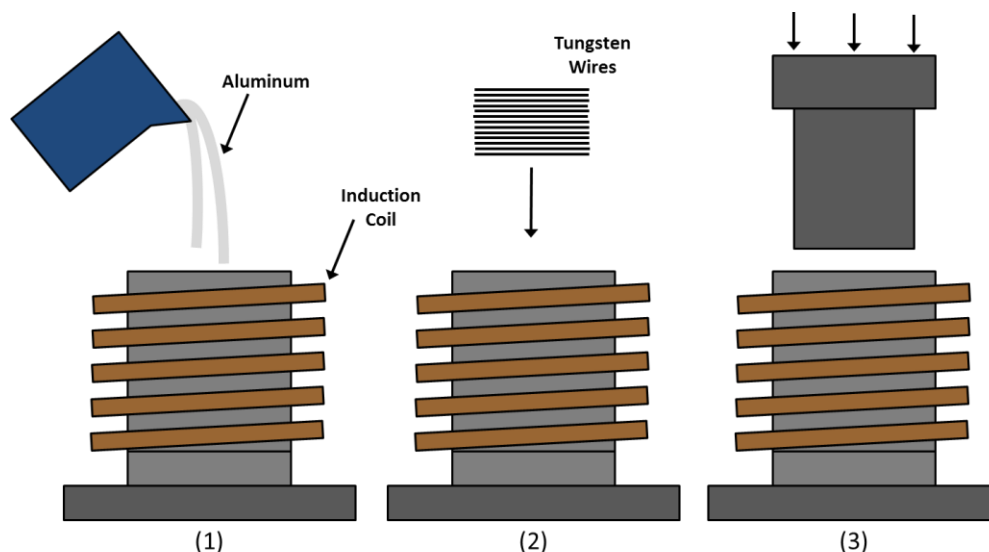


**Figure 18: Schematic of induction casting manufacturing process**

Even in the laboratory, this process moves relatively quickly, only taking a few minutes to heat both the tungsten and aluminum. Further details would be necessary to finalize the manufacturing plan, but the process shown here is a viable idea.

**Next Steps**
In the future, it is proposed to discover the full potential of increased density casings using tungsten wires. The metal-matrix, vertical wire configuration shows promise for readily disintegrating the aluminum in the casing and thereby increasing the amount of aluminum reaction. There are multiple parameters that can be explored in this area, such as the effects of wire length, wire diameter, and packing efficiency. A more tightly-toleranced mold would be designed to allow for higher pressure application during casting. Coating the wires with aluminum prior to casting may increase the amount of infiltration by essentially "pre-wetting" the surface of the tungsten wires. This technique may be possible through the use of sputter coating the tungsten surface with aluminum.

The tungsten spheres are an interesting option for increasing the density of the casings, but various obstacles must be overcome. Mainly, the cooling procedure for the dense sphere casings must be researched in order to aid in the prevention of dislocation formation along interfacial regions.

**II.B  Lower Energy States of Hydrogen**

**II.B.1 Background**
Existence of hydrogen in a fractional quantum state would have tremendous implications on science and technology, including energetic systems that bridge the gap between current chemical warheads and nuclear ones.   While there is appropriate skepticism over the theory and results, the publication of over thirty peer reviewed articles by Blacklight Power Inc. suggests that there are significant numbers of scientists who consider the concept at least possible.   Given that independent validation is a critical part of the scientific process, experiments directed at repeating these results in a separate facility may be justified.

The experiment chosen here was one in which a vacuum ultraviolet spectrum was produced in a gas by e-beam excitation.  Such a spectrum generated a regular series of lines that matched very closely the predicted rotational line spacing of the proposed di-hydrino molecule.   The spectrum had been independently observed by Ulrich, Wieser, and Murnick in an unrelated study at NJIT.   The NJIT group suggested oxygen as the source for these lines, but no atomic oxygen lines matched the observed pattern, though the spectral resolution of both studies was very low. Figure 19 below shows the BLP and NJIT spectra that we set out to examine.  The first step was to observe these spectra, but at a much higher level of resolution so that the underlying source could be better idenfied.
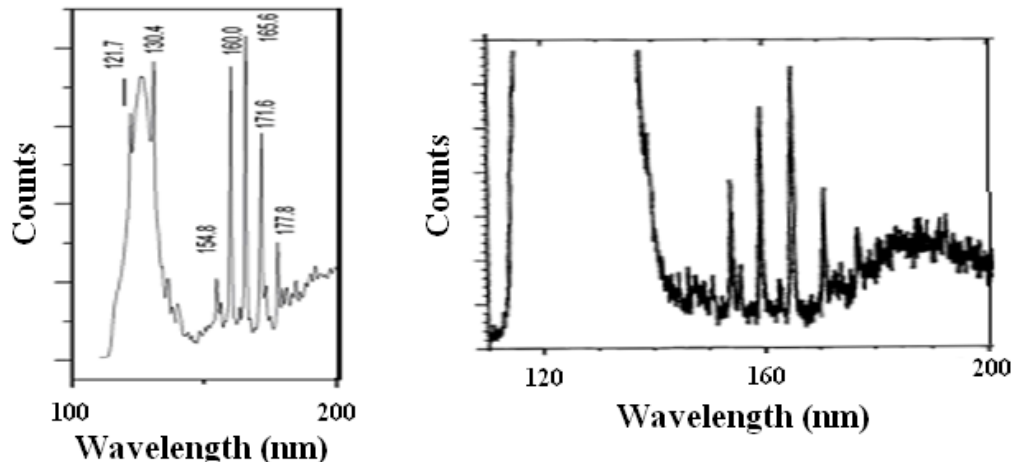
**Figure 20: Emission spectrum from an atmospheric pressure Ar gas with trace hydrogen excited by electron beam incident on the gas thru a SiN membrane. Both results are peer reviewed and independent. Left: from BLP Right: from Ulrich, Wieser, and Murnick at NJIT.**

### II.B.2 Experimental

An experimental apparatus was constructed to replicate the spectra. This apparatus, shown schematically in Figure 21 consisted of several key components including spectrometer, detector system, e-beam apparatus, test chamber, and associated electronics. These are covered in greater detail in the following paragraphs.
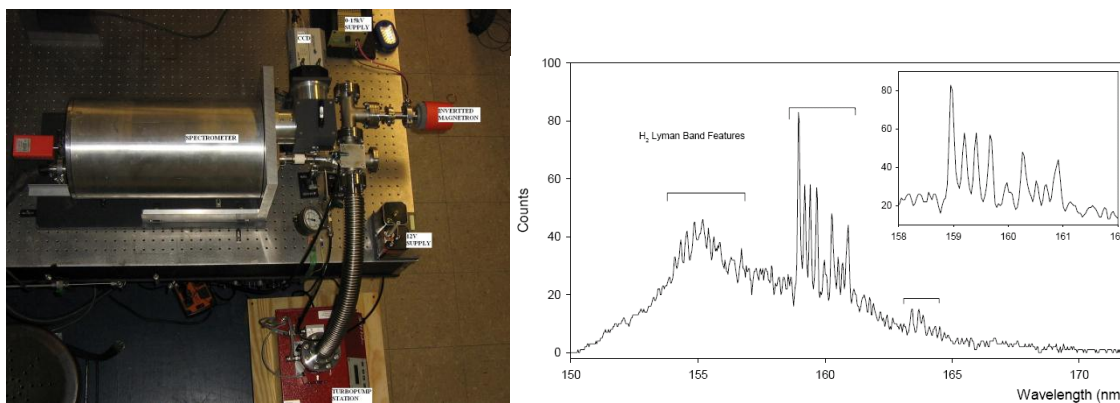


**Figure 21: Current experimental setup (left) including VUV spectrometer with array detector, high vacuum system with turbopump, and 12.5 kV electron beam source. Right: a spectrum of 3% H2 in Ar, showing the Lyman bands of H2 in the target range (150 – 175 nm).**

The vacuum spectrometer was a custom instrument designed and built here at UIUC. Though low cost was the primary driver behind making the instrument

ourselves, the additional advantage was that it significantly outperforms most commercial instruments.  A cylindrical housing contains the Czerny-Turner optical configuration, allowing for operation at $10^{-4}$ Torr and below.  The mirrors are off-axis parabaloids of 275 mm focal length, custom coated by Pellham Research for VUV reflectivity.  The grating is a 150 nm blazed 50 mm square grating from Richardson with Al-MgF$_2$ overcoat.  A variable inlet slit sits inside the chamber, and light enters through an MgF$_2$ window.  The superb optics in this system allow for excellent imaging characteristics and sharp lines at the exit focal plane.  The resolution with the 2400 gr/mm grating in first order is approximately 0.1 nm in first order and 0.05 nm in second order, with ranges of 30 nm in first order and 15 nm in second order.

The detector was selected to be a VUV intensifier made by Photonis, and it consisted of a CaF$_2$ window, two stage, 18 mm MCP, and phosphor output.  This detector was placed inside the chamber, and the phosphor imaged through a glass window onto an external CCD detector from Andor.  The CCD detector could be deep cooled for long exposures.

The e-beam setup was replicated from BLPs work after several interactions with the company.  Many of the details of the setup were not listed in the papers.  The 'e-beam' was simply a TV tube electron gun with all cathodes, deflecting plates, and other hardware removed, leaving only the filament source and Wehnelt cap.  The chamber was biased at negative HV (-15kV), and the filament and cap were all at ground.  An isolated battery powered supply of 18V with a potentiometer was assembled and used to control the voltage to the filament during testing.  A small magnet on the side of the tube in which the filament resided was critical for directing the electrons onto the aperture.

The aperture was an SiN membrane from SPI, and it was roughly 100 nm thick and 1 mm square.  It was glued onto a hole in a flange using vacuum epoxy.  The filament chamber was kept at $10^{-5}$ – $10^{-6}$ Torr via a turbopump system.  Between the aperture and MgF$_2$ input window of the spectrometer was a small test chamber isolated from the spectrometer by a ceramic vacuum break.  A CaF$_2$ lens focused emission from near the aperture onto the inlet slit.  The chamber was connected to bottles of various gases including UHP Ar, UHP H$_2$, commercial Ar, and a 3% H$_2$ in Ar mixture.

## II.B.3 Spectroscopic Results
Figure 22 below shows a spectrum generated by the system from a fill of UHP Ar at approximately 1 atm.  Exposures of up to 5 min were required to obtain good SNR.  Eventually, all major lines observed by BLP were observed in our setup, but at much higher resolution allowing us to better identify line positions and shapes.
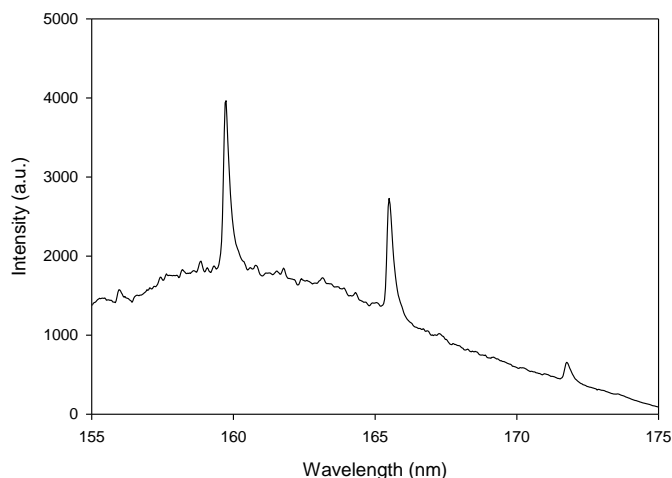
**Figure 22:  A spectrum of UHP argon under -15kV electron excitation through a SiN aperture.  The three features match those observed at BLP and NJIT.**

For calibration, a silicon/aluminum laser discharge generated 15 lines, and each line agreed in the fit to better than 1/3 pixel, or 0.01 nm.  For the upper wavelength range, I used a selenium hollow cathode lamp and got 6 good lines with the same precision of the fit.   A summary of my results and a plot of the line positions is shown below.

| Postulated Line | Line Pos'n BLP (nm) | Line Pos'n UIUC (nm) |
|---|---|---|
| P(1) | 154.8 | 154.47 |
| P(2) | 160.0 | 159.74 |
| P(3) | 165.6 | 165.34 |
| P(4) | 171.6 | 171.26 |
| P(5) | 177.8 | 177.55 |

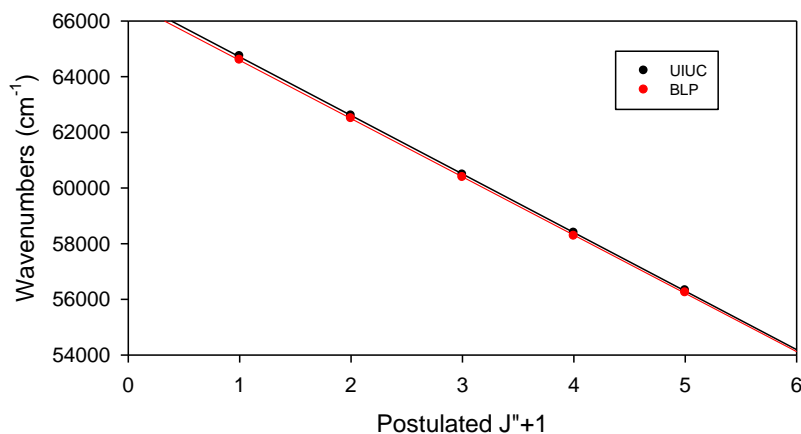| Fit data: | BLP | UIUC |
|---|---|---|
| Vibrational Constant (eV) | 0.5167 | 0.5178 |
| Rotational Constant (eV) | 0.01622 | 0.01630 |
| $r^2$ | 0.9999484 | 0.9999572 |



**Figure 23:  A plot of the observed line positions against postulated rotational states.**

*Any opinions expressed in this document are those of the author alone and do not necessarily represent the opinions of the University of Illinois or DTRA.*

The agreement was very good.  BLP's results (as well as those from NJIT) were clearly validated, and an increase of resolution of 10x continued to show the linearity of the distribution of line positions.  Indeed, our regression yielded a slightly higher $r^2$ value than BLPs.

There were two noteworthy observations, however.  First, the lines did appear to have some possible structure that may suggest these were not isolated lines but bands instead.  Second, the spectra were obtained with only argon added to the system.  Any H would have to be from an impurity.  Attempts to add even trace amounts of H resulted in the loss of the observed signal and the dominance of the well known Lyman band emission.

A final set of experiments was performed in which the system was operated in second order to double the resolution.  The results are shown in Figure 24.  Atomic lines, most likely Ar II lines were observed in first order, breaking through the bandpass filter at around 309 nm.  These lines show the system resolution and how narrow isolated lines would appear.   The feature at 159.74 nm is clearly a broadened feature, much larger than a single line, with an asymmetric structure suggesting a red-degraded band.
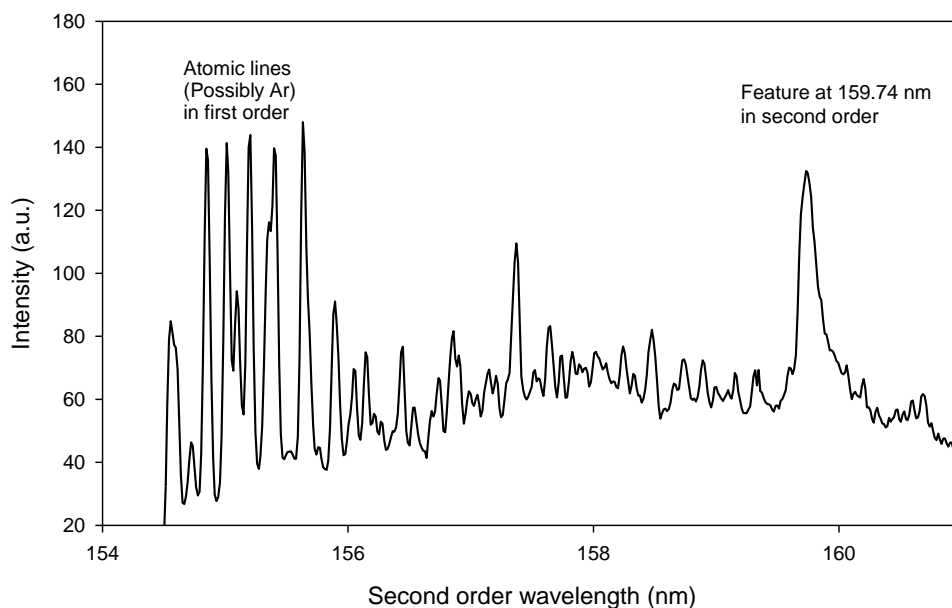


**Figure 24:  A second order scan in the vicinity of the feature at 159.74 nm.  The observed feature is clearly wider than an atomic line and has a red-degraded structure.**

Furthermore, additional analysis located several papers discussing CO 4th positive band emission from e-beam excitation.  Under these conditions, direct excitation by electron impact to an upper state likely produces no change in vibrational state, so

the band emissions with v'=0 are most likely to be strongest. Additionally, CO 4th positive bands are red degraded. A comparison of the band locations of these bands to the features is shown in the table below. It is unambiguously clear that the features observed in our experiments, as well as those from BLP and NJIT works are CO 4th positive emission and not di-hydrino or oxygen.

| CO Band | Calculated Position (nm) | My Measurement (nm) |
|---------|--------------------------|----------------------|
| (0,0) | 154.44 | 154.47 |
| (0,1) | 159.73 | 159.74 |
| (0,2) | 165.32 | 165.34 |
| (0,3) | 171.24 | 171.26 |
| (0,4) | 177.51 | 177.55 |

**II.B.4 Conclusions and Implications**

The spectrum presented by BLP is not the di-hydrino. It is due to a common molecule with a known vacuum ultraviolet spectrum. These features were misidentified in both BLP and NJIT publications. While this assignment is incorrect, hydrino theory is not disproven by our experiments. This spectrum is only a very small part of the BLP case, a secondary point at best. The excess heat and energy are their key points.

Several recent results from BLP have provided additional evidence for the existence of the hydrino and dihydrino. These include excess heat results from their electrochemical cell, as well as Raman spectra with peaks corresponding to supposed di-hydrino rotational lines. The Raman peaks are particularly surprising and difficult to assign to anything else. In the author's opinion, these would be interesting topics for a future study, provided anyone is still interested.

# III. Funding Profile from FY04-12

For this project, $99,823 was allocated for the period of 20 April 2012 to 30 October 2012.

# IV. What needs to happen so that Advanced Energetics can meet its goal of achieving 10-fold improvement over TNT? How can this work help?

A significant fraction of the 10x can be achieved through reactive casings. If case mass is two-thirds of the total mass, and 8 kJ/g can be realized from an RM case (which is not an unreasonable number. Al is 31 kJ/g, and so even 25% efficiency on

a pure Al case reaches 8 kJ/g), then 5X TNT is achieved. Approaches such as the reactive case approach pursued in this work have the promise to reach these levels, and the casting technologies we're investigating may be able to make such technologies affordable.

Energetics based on postulated hydrino states would easily reach better than 10x TNT, but proof of the existence of such states would necessarily need to precede any energetics development.

## V. Future funding needs, FY14-18 for achieving the above goal.

Based on our experience from just six months of work in 2012, it seems likely that with a full year of additional development at the level of $100,000 for the year, we could achieve cases with densities in the range of 12 g/cc, with conversion efficiencies for aluminum in the vicinity of 30%. Higher densities and efficiencies may be possible using more extensive modifications of the technique.

**DEPARTMENT OF DEFENSE**

DEFENSE TECHNICAL
INFORMATION CENTER
8725 JOHN J. KINGMAN ROAD,
SUITE 0944
FT. BELVOIR, VA  22060-6201
      ATTN: DTIC/OCA

DEFENSE THREAT REDUCTION
AGENCY
8725 JOHN J. KINGMAN ROAD
STOP 6201
FT. BELVOIR, VA  22060-6201
      ATTN: S. PEIRIS

**DEPARTMENT OF DEFENSE**
**CONTRACTORS**

EXELIS, INC.
1680 TEXAS STREET, SE
KIRTLAND AFB, NM  87117-5669
      ATTN: DTRIAC